CONF-851113--5

CONF-851113--5

DE86 006096

ASPECTS OF THE DOSIMETRY OF RADIONUCLIDES WITHIN THE SKELETON WITH PARTICULAR EMPHASIS ON THE ACTIVE MARROW

K. F. Eckerman
Health and Safety Research Division
Oak Ridge National Laboratory
P. O. Box X
Oak Ridge, Tennessee 37831

ASPECTS OF THE DOSIMETRY OF RADIONUCLIDES WITHIN THE SKELETON WITH PARTICULAR EMPHASIS ON THE ACTIVE MARROW

K. F. Eckerman
Health and Safety Research Division
Oak Ridge National Laboratory
P. O. Box X
Oak Ridge, Tennessee 37831

ABSTRACT

Epidemiological surveys on man and results from animal experiments have shown that two tissues associated with the skeleton are of primary concern with respect to cancer induction by ionizing radiation. These are the cells on or near endosteal surfaces of bone, from which osteosarcomas are thought to arise, and hematopoietic bone marrow, which is associated with leukemia. The complex geometry of the soft tissue-bone intermixture makes calculations of absorbed dose to these target regions a difficult problem. In the case of photon or neutron radiations, charged particle equilibrium may not exist in the vicinity of soft tissue-bone mineral interface. In this paper a general study of the dosimetry of radionuclides within the skeleton is presented. Dosimetric data consistent with the MIRD schema and reflecting the physical and anatomical parameters defining the energy deposition are tabulated for the relevant target regions.

INTRODUCTION

Calculation of absorbed dose in the tissues of the skeleton is a complex problem because charged particle equilibrium may not exist within the vicinity of soft tissue-bone mineral interfaces. Treatment of this problem has been hampered by difficulties in modeling the microscopic-intricate intermixture of soft tissue and bone. Most estimates of absorbed dose in organs of the body from photon radiation are based on transport calculations made for a mathematical analogue of the body with a homogeneous representation of the skeleton (1-3). While the homogeneous skeleton is adequate for transport considerations (i.e., appropriate scatter and absorption properties are assigned), the accompanying assumption of charged particle (electronic) equilibrium is often not satisfied

in skeletal tissues. The transport of energy by secondary electrons must be considered in deriving realistic estimates of absorbed dose in soft tissues close to bone mineral, in particular the active marrow.

This problem was first studied in 1949 by Spiers (4) and later by Spiers and others (5-9) using simple geometrical models (e.g., thin slabs, cylinders, and spherical cavities) to approximate the interface geometry. These studies demonstrated that for photon energies less than about 200 keV, electronic equilibrium does not exist and electrons liberated in mineral regions may contribute significantly to the absorbed dose in soft-tissue regions of the skeleton. Snyder et al. encountered the intractable geometry of trabecular bone in their Monte Carlo studies of photon transport and elected to formulate their calculation of absorbed dose in marrow in a conservative manner (1). They partitioned the total energy deposition in the homogeneous skeleton among various skeletal tissues, including active marrow, using skeletal mass fractions. The potential for an overestimate of absorbed dose in the active marrow was noted (see pp. 20 of Ref. 1):

> "... it is assumed that the marrow absorbs energy per gram as efficiently as does bone. This assumption is not grossly wrong at energies of 200 keV or more, but is increasingly inaccurate at energies below 100 keV. The effect is to somewhat overestimate the dose to marrow and to somewhat underestimate the dose to bone. This difficulty results from the failure to find ways to program the intricate mixture of bone and marrow spaces in a more realistic fashion."

The potential overestimate has been considered by Rosenstein (3), Kramer (10), Ashton and Spiers (11), and Kerr (12), who indicate that for photon energies less than 100 keV the error is 300% or more. Rosenstein and Kramer apply an energy-dependent correction factor to values computed using the homogeneous skeleton. The correction factor assumes electronic equilibrium (marrow is considered to be a small cavity in the homogeneous skeleton) and includes consideration of the enhancement due to photoelectrons from bone, as indicated by Spiers (13). No computational approach existed which formulated the absorbed dose to the skeletal tissues at risk in terms of the relevant physical and anatomical variables defining the energy deposition.

The problems in formulating the absorbed dose in the active marrow from photon radiation are similar to those encountered in the dosimetry of beta emitters incorporated in bone. For beta emitters Spiers and co-workers reduced the intractable three dimensional geometry to one dimension through use of measured distributions of chord-lengths in trabeculae and marrow cavities of trabecular bone (14-16). Clearly this approach to the geometry can be applied to secondary electrons liberated by photon interactions in the skeleton.

THE DISTRIBUTION OF CELLS AND TISSUES OF THE SKELETON AT RISK

The skeleton is a complex structure composed of bone, yellow or fatty marrow, red or active marrow, and assorted connective tissues. Throughout the discussion, "bone" refers to the skeletal mineral and adjacent cells and fluid remaining when the skeleton is stripped of its cartilage, periarticular tissue, and marrow. Bone can be divided into two categories, structural bone and metabolic bone. "Structural" refers to the mechanical function of the skeleton, while "metabolic" refers to the role the bone mineral plays in regulating the extracellular calcium levels, particularly in blood plasma.

In the mature skeleton, two bone types are reasonably distinct in terms of appearance as well as retention of bone seekers (17-19). Cortical bone is the hard, compact bone found largely in the shafts of the long bones. Trabecular bone, sometimes referred to as cancellous bone, is the soft, spongy bone composed of a lattice-work of fragile appearance and located at the interior of the flat bones and the ends of the long bones. In general, cortical and trabecular bone may be distinguished in terms of their surface-to-volume ratios, which are usually about 4 times larger for trabecular bone. Cortical bone constitutes about four-fifths, or about 4 kg, of the skeletal mineral in the mature skeleton while the remaining fifth or 1 kg is associated with trabecular bone (17). The high surface-to-volume ratio of trabecular bone arises from the interlacing splinters of bone (trabeculae) which form cavities in which the active marrow is found. The dominant microscopic structure of cortical bone is the Haversian system or osteon, which is a roughly cylindrical volume or canal containing blood vessels, osteoblasts (bone-forming cells), and undifferentiated cells. These canals are typically 50 microns in diameter (17) and, with their supporting channels, serve to supply nutrients to the interior of cortical bone.

There is now general agreement that two cell populations in the skeleton are at risk, namely, the hematopoietic stem cells of marrow and the osteogenic cells of the skeleton, particularly those on the endosteal surfaces of bone (18). Since blood cells are found in various stages of maturation within the active marrow, this tissue is of primary concern as the target tissue with respect to induction of leukemia. The osteogenic cells are the precursors of osteoblasts, which are involved in the formation of new bone, and osteoclasts, which are involved in the resorption of bone. Thus, osteogenic cells constitute the target tissue of concern with respect to induction of bone cancer. Committee 2 of the ICRP (20) has assumed that the hematopoietic stem cells are uniformly distributed within the marrow space of trabecular bone, and the dose equivalent in these cells is taken as the average dose equivalent in the marrow

space. For the osteogenic cells, the Committee now recommends that the dose equivalent be calculated as an average over endosteal tissues up to a distance of 10 μm from bone surfaces (20). Since cortical and trabecular bone contribute about equally to the skeletal surface area, half of the endosteal tissues are assumed to be associated with trabecular bone and half with cortical bone (17). The dose to the osteogenic cells is usually referred to as the bone surface dose, but this is a misnomer since the dose calculation is actually made for the mass of soft-tissue within 10 μm of the interface between bone and soft tissue, rather than for just the bone surface.

ABSORBED FRACTION DATA FOR ELECTRONS IN TRABECULAR BONE

Because the structure of trabecular bone cannot be described in simple geometrical terms, Spiers (13,21-22) introduced a method of calculating the energy deposition in which the geometries of the trabeculae and marrow cavities are represented by the distributions of chord-lengths across them. The chord-length distributions for trabeculae and marrow cavities were obtained by optically scanning the trabeculation under conditions of μ-randomness (the different types of randomness are discussed in a paper by Eckerman et al. in this proceedings). If the track of a particle through each trabecula and cavity is assumed to be straight, then the total track in trabeculation can be approximated by alternating chord-lengths in trabeculae and cavities selected randomly from the measured distributions.

DISTRIBUTION OF CHORD-LENGTHS

Measurements of the chord-length distributions in trabecular bone for up to nine bones in several species (15, 16, 23) have been reported by the Bone Dosimetry Research Unit, University of Leeds, UK, under the direction of Professor Spiers. Mean chord- and ray-lengths for the trabeculae and marrow cavities of several trabecular bones of the skeleton of man are summarized in Table 1. The chord distributions for the lumbar vertebra and the parietal bone are shown in Fig. 1. Note that the parietal bone of the adult skeleton appears to be distinct from other trabecular bones as suggested by ratios of mean chord-lengths given in Table 1.

The chord distributions were measured under μ-randomness and thus correspond to the pathlength of radiation incident on the regions in an isotropic manner. For particles orginating with the marrow space and the trabeculae the relevant randomness is I-randomness. It has been shown that the distributions for μ- and I-randomness are related, in general, as (24):

Table 1. Mean chord- and ray-lengths (μm) for trabeculae and marrow cavities in various bones of man

Bones	Trabeculae[a]			Marrow Cavities[a]			Ratio of mean chord lengths
	$\langle t \rangle_\mu$	V_μ	$\langle t \rangle_i$	$\langle l \rangle_\mu$	V_μ	$\langle l \rangle_i$	$\langle t \rangle_\mu : \langle l \rangle_\mu$
44-year-old male[b]							
Parietal	511	0.570	401	389	0.784	347	1.31
Cerival vertebra	279	0.719	240	910	0.894	861	0.307
Lumbar vertebra	247	1.11	260	1228	1.12	1299	0.201
Rib	265	1.49	330	1706	1.09	1786	0.155
Iliac crest	242	0.675	203	904	0.647	745	0.268
Femur head	232	0.665	193	1157	0.901	1099	0.200
Femur neck	314	0.914	301	1655	0.905	1576	0.190
9-year-old child[c]							
Parietal	539			306			0.272
Cerival vertebra	162			906			0.179
Lumbar vertebra	168			857			0.196
Rib	231			1123			0.204
Iliac crest	180			744			0.242
Femur head & neck	249			616			0.404
20-month-old child[b]							
Parietal bone	566	1.21	625	255	2.90	500	2.22
Lumbar vertebra	188	1.04	192	736	0.987	731	0.255
Rib	191	1.22	212	559	1.04	569	0.342
Iliac crest	181	1.43	206	575	0.873	539	0.315
Femur	197	0.865	184	789	1.10	830	0.250

a) Notation: ($\langle t \rangle_\mu$, V_μ) and ($\langle l \rangle_\mu$, V_μ) denote the mean and the fractional variance under μ-randomness for the trabeculae and marrow cavities, respectively. $\langle t \rangle_i$ and $\langle l \rangle_i$ denote the mean ray-length for trabeculae and cavities, respectively. Lengths are in units of μm.

b) Values were computed from the chord-length distributions of Ref. 23.

c) See Ref. 15.

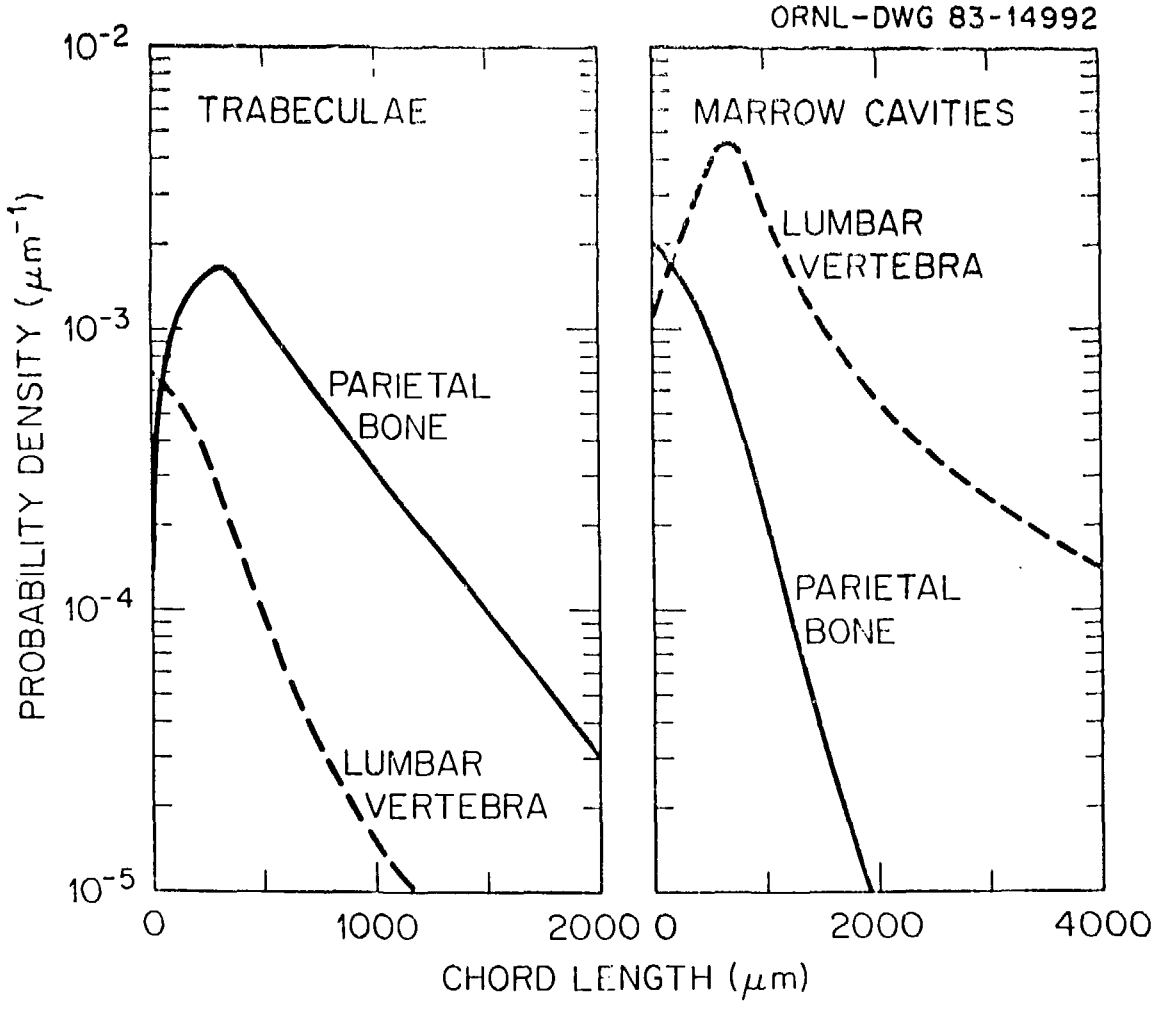

Figure 1. Illustration of measured chord-length distributions for μ-randomness in the trabeculae (left) and marrow cavities (right) of the lumbar vertebra and parietal bone from a 44-year-old male.

$$f_I(x) = \frac{x}{\langle x \rangle_\mu} f_\mu(x) \quad , \tag{1}$$

where

$f_I(x)$ and $f_\mu(x)$ denote the probability density functions for chord-lengths under I- and μ-randomness, respectively,

$\langle x \rangle_\mu$ denotes the mean value of the $f_\mu(x)$ distribution.

Eq. 1 refers to the full chord; however, we are interested in "half" chords or rays formed by particles originating inside the convex body. A chord of length x, selected from $f_I(x)$, will give rise to rays whose lengths are uniformly distributed between 0 and x, i.e., any point on the chord could serve to define the ray. Thus the chord distribution under μ-randomness and Eq. 1 allows selection of the path-lengths needed to simulate the path of particles within trabecular bone.

COMPUTATIONAL METHOD FOR ESTIMATING ABSORBED FRACTIONS

The absorbed fraction in target region r_k of radiation energy emitted within source region r_h is defined as the energy imparted to r_k divided by the total energy emitted in r_h. Thus $\phi(r_k \leftarrow r_h)$ embodies the transport of the radiation under consideration as well as the geometric relationship of the source and target regions. The absorbed fraction data presented here are for monoenergetic electrons emitted uniformly (by mass) and isotropically within the trabeculae and cavities of trabecular bone. The target regions of interest are the red (active) marrow, for which we average the energy deposition over the marrow cavities, and the endosteal tissues within 10 μm of the surfaces of bone.

The representation of a typical path of an electron of energy E and range in marrow R_{RM} are illustrated in Fig. 2. By use of chord-length distributions the three-dimensional geometry has been reduced to one dimension. Furthermore, the two media considered in the problem (bone and marrow) can be reduced to a single medium as the ratio of the range of electrons in marrow, R_{RM} to that of bone, R_{TB} is nearly constant over electron energies of interest here, that is,

$$\frac{R_{RM}}{R_{TB}} \cong 1.75 \quad . \tag{2}$$

For irradiation of the active marrow by electrons orginating within trabeculae, Monte Carlo sampling is used to select a chord-length, t, from the probability density function, $f_I(t)$, for the bone under consideration. A ray-length, t', is

ORNL-DWG 83-14258

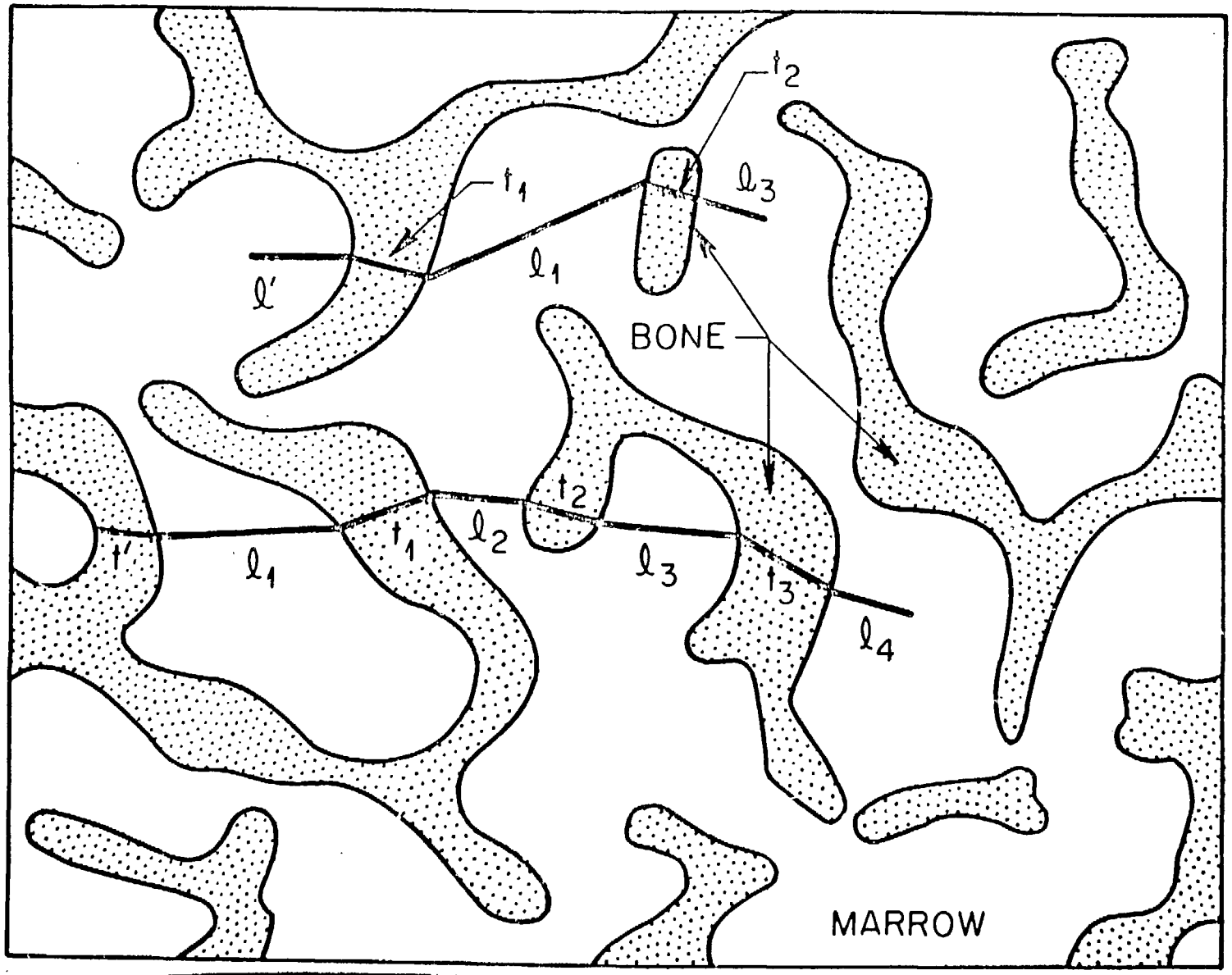

Figure 2. Illustration of typical tracks for electrons originating in trabecular bone (bottom) and marrow cavities (top).

then determined as $t' = \xi\, t$, where ξ is a random number uniform on the region $0 < \xi < 1$. The electron is tracked as it alternately passes through marrow cavities along lengths l_1, l_2, ..., and trabeculae along chords t_1, t_2, ..., selected by Monte Carlo sampling of the probability density functions $f_\mu(l)$ and $f_\mu(t)$, respectively. The electron is tracked until

$$1.75(t' + t_1 + t_2 + \ldots) + (l_1 + l_2 + \ldots) \geq R_{RM} \quad , \tag{3}$$

i.e., all of its energy has been deposited. The energy deposition in trabeculae (t's) and marrow cavities (l's) is calculated as the difference between the energy on entering and leaving a trabecula or cavity, in each case being determined from the residual range of the electron at that point in its track. The range-energy relationship was taken from Berger (25). By tracking a large number of electrons in this manner the absorbed fraction, $\varphi(RM \leftarrow TB)$, is obtained by dividing the total energy deposited in marrow cavities by the total energy of electrons simulated.

For electrons emitted within marrow cavities, the calculations proceed as above with selection of a chord-length from the probability density function $f_I(l)$ and determination of a ray-length l' as noted above. The electron is tracked until

$$(l' + l_1 + l_2 + \ldots) + 1.75(t_1 + t_2 + \ldots) \geq R_{RM} \quad . \tag{4}$$

The energy deposition in trabeculae and marrow cavities and the absorbed fraction, $\varphi(RM \leftarrow RM)$, are determined as discussed above. Typically ten to seventy thousand electrons were tracked in each of the calculations of the absorbed fraction. The statistical errors in the Monte Carlo calculations were less than 1% in each case.

The absorbed fraction data for the parietal bone and lumbar vertebra of the skeleton of a 44-year old male are shown in Fig. 3. At low electron energies, $\varphi(RM \leftarrow TB)$ approaches zero and $\varphi(RM \leftarrow RM)$ approaches unity. This limiting behavior reflects the fact that at low energy the range of electrons is small relative to the mean ray-lengths, $\langle t \rangle_i$ and $\langle l \rangle_i$, and thus the energy is locally deposited. At high energies, $\varphi(RM \leftarrow RM) \cong \varphi(RM \leftarrow TB)$ and the behavior is described as

$$\lim_{E \to \infty} \varphi(RM \leftarrow TB) \cong \varphi(RM \leftarrow RM) \cong \frac{\langle l \rangle_\mu}{\langle l \rangle_\mu + 1.75\langle t \rangle_\mu} \quad , \tag{5}$$

i.e., the absorbed fraction is simply the fractional track length in the

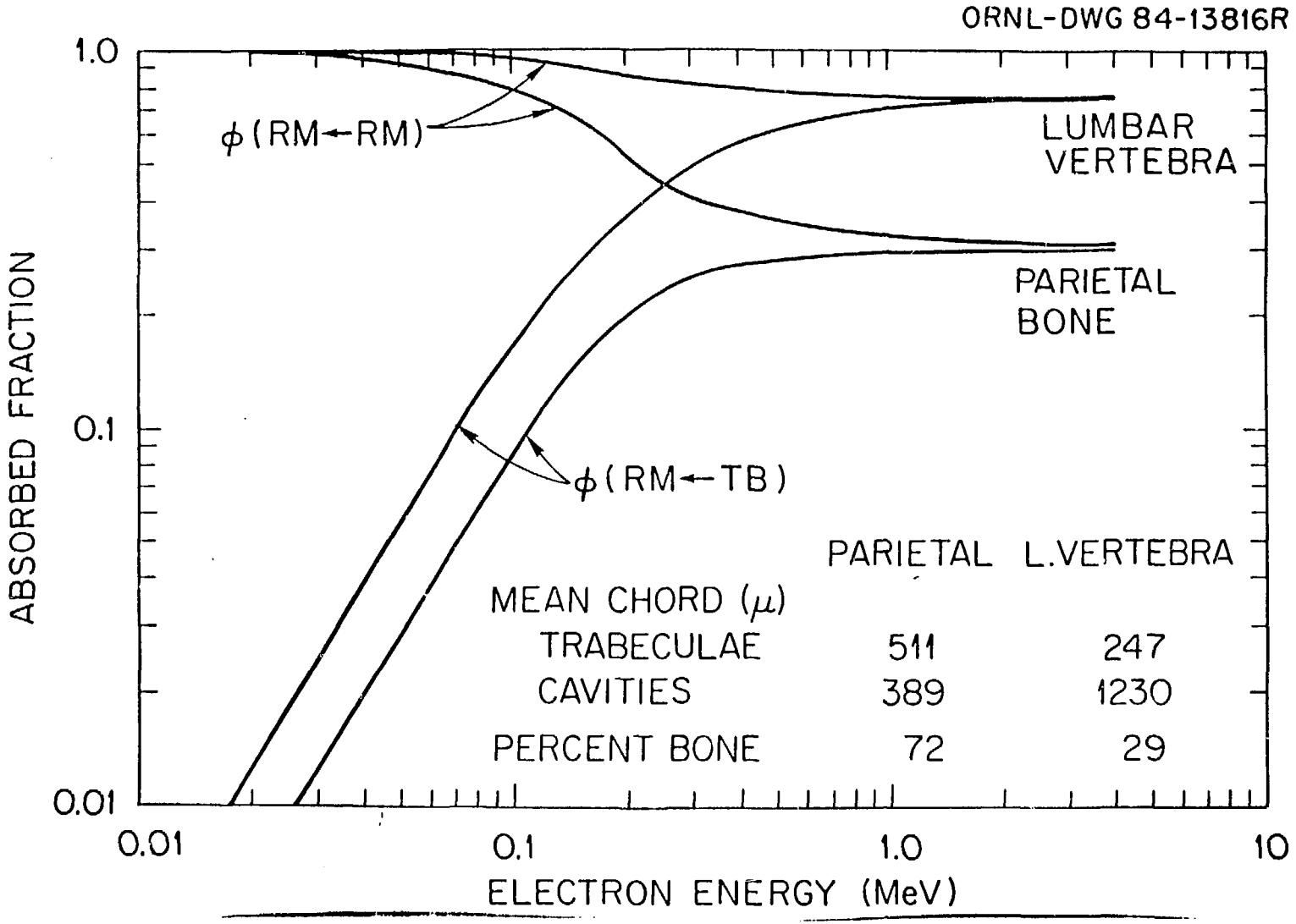

Figure 3. Absorbed fractions for active marrow from monoenergetic electrons emitted uniformly in the trabeculae, $\phi(RM \leftarrow TB)$, and active marrow, $\phi(RM \leftarrow RM)$, of lumbar vertebra and parietal bone from the skeleton of a 44-year-old male.

marrow cavities. The equality of the absorbed fractions at high energy arises as electrons traverse multiple trabeculae and cavities, thus establishing an energy deposition pattern which is largely independent of the electron's origin.

The complete results of the calculations for the parietal bone of the skull and the lumbar vertebra are given in Tables 2 and 3 for a 44-year old male and a 20-month old child, respectively. Although rather sharp distinctions are evident in the absorbed fraction data between the parietal bone and lumbar vertebra of either the child or the adult, the distinction with age is less pronounced. Further tabulation of the age dependence of various parameters characterizing the skeleton is given in Table 4.

ABSORBED DOSE PER UNIT PHOTON FLUENCE

In the anthropomorphic phantom the skeleton is represented as a uniform mixture of its component tissues, namely, cortical bone, trabecular bone, fatty marrow, active (hematopoietic) marrow, and osteogenic cells adjacent to the surfaces of both cortical and trabecular bone ("bone surface"). To estimate the energy deposition in these regions by photons, one must consider the energy transport by secondary electrons arising from photon interactions within the regions and from electrons entering the regions from skeletal components in the immediate vicinity of the target, e.g., bone adjacent to the target.

Consider the trabeculation of a bone experiencing a fluence, $\Phi(E)$, of photons of energy E. Let m(TB), m(RM), and m(BS) denote the mass of bone (trabeculae), marrow, and endosteal tissue adjacent to the surface of the trabeculation. If we index the type of interaction by i and the region in which it occurred by r, r = TB or RM, then the absorbed dose in active marrow, D(RM), and in the endosteal tissue, D(BS), per unit fluence can be expressed as

$$\frac{D(RM)}{\Phi(E)} = \sum_r \frac{m(r)}{m(RM)} \sum_i \int_0^\infty \varphi(RM \leftarrow r, T_i)\ (i/\rho)_r\ n_r(T_i)\ T_i\ dT_i \qquad (6)$$

$$\frac{D(BS)}{\Phi(E)} = \sum_r \frac{m(r)}{m(BS)} \sum_i \int_0^\infty \varphi(BS \leftarrow r, T_i)\ (i/\rho)_r\ n_r(T_i)\ T_i\ dT_i \qquad (7)$$

where

$\varphi(RM \leftarrow r, T_i)$ is the absorbed fraction in RM from r for electrons of energy T_i,

$(i/\rho)_r$, i = τ, σ, and k, denotes the mass attenuation coefficients in medium r for the photoelectric, Compton, and pair-production interactions, respectively,

Table 2. Absorbed fraction, ϕ, in active marrow, RM, and bone surface, BS, from a uniformly distributed source of monoenergetic electrons in trabeculae, TB, and marrow of the parietal bone and lumbar vertebra of a 44-year-old male.

Electron energy (MeV)	Parietal bone				Lumbar Vertebra			
	ϕ(RM ← TB)	ϕ(RM ← RM)	ϕ(BS ← RM)	ϕ(BS ← TB)	ϕ(RM ← TB)	ϕ(RM ← RM)	ϕ(BS ← RM)	ϕ(BS ← TB)
0.010	1.95(-3)	0.994	1.05(-1)	1.95(-3)	3.94(-3)	0.999	3.87(-2)	2.94(-3)
0.015	3.29(-3)	0.990	9.67(-2)	3.29(-3)	7.81(-3)	0.997	3.77(-2)	6.56(-3)
0.020	5.77(-3)	0.983	9.11(-2)	5.77(-3)	1.29(-2)	0.996	3.51(-2)	1.17(-2)
0.030	1.23(-2)	0.969	7.88(-2)	1.14(-2)	2.59(-2)	0.991	3.06(-2)	2.08(-2)
0.040	1.98(-2)	0.950	6.97(-2)	1.54(-2)	4.34(-2)	0.985	2.82(-2)	2.90(-2)
0.050	2.94(-2)	0.927	6.55(-2)	1.85(-2)	6.26(-2)	0.979	2.75(-2)	3.32(-2)
0.060	4.03(-2)	0.901	6.10(-2)	2.04(-2)	8.25(-2)	0.971	2.68(-2)	3.56(-2)
0.080	6.34(-2)	0.854	5.28(-2)	2.18(-2)	1.31(-1)	0.953	2.51(-2)	3.91(-2)
0.10	8.80(-2)	0.794	5.09(-2)	2.37(-2)	1.83(-1)	0.935	2.58(-2)	4.24(-2)
0.15	1.53(-1)	0.654	4.52(-2)	2.65(-2)	3.12(-1)	0.888	2.82(-2)	4.24(-2)
0.20	1.99(-1)	0.538	4.08(-2)	2.84(-2)	4.17(-1)	0.848	2.78(-2)	3.87(-2)
0.30	2.58(-1)	0.415	3.87(-2)	2.98(-2)	5.47(-1)	0.808	2.84(-2)	3.44(-2)
0.40	2.71(-1)	0.376	3.60(-2)	2.96(-2)	5.97(-1)	0.793	2.90(-2)	3.23(-2)
0.50	2.76(-1)	0.358	3.50(-2)	3.00(-2)	6.25(-1)	0.779	2.86(-2)	3.32(-2)
0.60	2.82(-1)	0.346	3.35(-2)	3.05(-2)	6.48(-1)	0.767	2.85(-2)	3.30(-2)
0.80	2.88(-1)	0.335	3.37(-2)	3.09(-2)	6.74(-1)	0.765	2.87(-2)	3.32(-2)
1.0	2.93(-1)	0.327	3.30(-2)	3.09(-2)	6.90(-1)	0.757	2.88(-2)	3.23(-2)
2.0	2.97(-1)	0.317	3.19(-2)	3.11(-2)	7.17(-1)	0.747	2.94(-2)	3.26(-2)
3.0	3.00(-1)	0.311	3.18(-2)	3.11(-2)	7.22(-1)	0.747	2.90(-2)	3.23(-2)
4.0	3.01(-1)	0.308	3.15(-2)	3.11(-2)	7.27(-1)	0.744	2.88(-2)	3.22(-2)

Table 3. Absorbed fraction, ϕ, in active marrow, RM, and in bone surface, BS, from a uniformly distributed source of monoenergetic electrons in the trabeculae, TB, and marrow space of the parietal bone and lumbar vertebra of a 20-month old child.

Electron energy (MeV)	Parietal Bone				Lumbar Vertebra			
	ϕ(RM ← TB)	ϕ(RM ← RM)	ϕ(BS ← TB)	ϕ(BS ← RM)	ϕ(RM ← TB)	ϕ(RM ← RM)	ϕ(BS ← TB)	ϕ(BS ← RM)
0.01	1.62(-3)	0.990	1.62(-3)	1.40(-1)	4.66(-3)	0.997	4.66(-3)	5.99(-2)
0.015	3.44(-3)	0.981	3.44(-3)	1.33(-1)	9.90(-3)	0.995	9.90(-3)	5.68(-2)
0.02	6.09(-3)	0.969	6.09(-3)	1.21(-1)	1.65(-2)	0.992	1.65(-2)	5.26(-2)
0.03	1.24(-2)	0.947	1.14(-2)	1.01(-1)	3.39(-2)	0.984	3.16(-2)	4.62(-2)
0.04	1.91(-2)	0.920	1.47(-2)	9.04(-2)	5.67(-2)	0.973	4.24(-2)	4.19(-2)
0.05	2.80(-2)	0.889	1.74(-2)	7.98(-2)	8.01(-2)	0.962	4.83(-2)	3.94(-2)
0.06	3.46(-2)	0.858	1.79(-2)	6.97(-2)	1.12(-1)	0.949	5.37(-2)	3.75(-2)
0.08	5.12(-2)	0.789	2.00(-2)	6.28(-2)	1.74(-1)	0.922	5.83(-2)	3.49(-2)
0.10	7.09(-2)	0.724	2.28(-2)	5.73(-2)	2.34(-1)	0.892	5.68(-2)	3.52(-2)
0.15	0.106	0.591	2.44(-2)	4.67(-2)	3.74(-1)	0.829	5.30(-2)	3.65(-2)
0.20	0.130	0.501	2.61(-2)	4.21(-2)	4.70(-1)	0.786	4.78(-2)	3.95(-2)
0.30	0.154	0.401	2.67(-2)	3.76(-2)	5.58(-1)	0.750	4.37(-2)	4.11(-2)
0.40	0.168	0.354	2.79(-2)	3.49(-2)	5.94(-1)	0.730	4.20(-2)	4.23(-2)
0.50	0.176	0.328	2.80(-2)	3.34(-2)	6.26(-1)	0.722	4.16(-2)	4.25(-2)
0.60	0.179	0.308	2.75(-2)	3.26(-2)	6.38(-1)	0.718	4.12(-2)	4.11(-2)
0.80	0.181	0.283	2.79(-2)	3.18(-2)	6.51(-1)	0.706	4.09(-2)	4.12(-2)
1.0	0.188	0.267	2.80(-2)	3.09(-2)	6.62(-1)	0.708	4.18(-2)	4.19(-2)
2.0	0.196	0.238	2.82(-2)	2.96(-2)	6.78(-1)	0.698	4.12(-2)	4.13(-2)
3.0	0.199	0.224	2.82(-2)	2.92(-2)	6.81(-1)	0.696	4.12(-2)	4.13(-2)
4.0	0.201	0.221	2.82(-2)	2.89(-2)	6.84(-1)	0.696	4.09(-2)	4.10(-2)

Table 4. Summary of descriptive parameters for the skeleton of man.

Descriptive Parameter	Age (yr) 0	1	5	10	15	Adult
Skeleton[1]						
Volume (cm^3)	288	813	1935	3309	5466	7155
Mass (kg)	0.351	1.138	2.709	4.633	7.652	10.0
Density (g/cm^3)	1.22	1.40	1.40	1.40	1.40	1.40
Bone mineral						
Calcium[2] (g)	28	99.8	219	396	806	1000
Mass[3] (kg)	0.140	0.499	1.095	1.980	4.030	5.000
Fraction[4]	0.399	0.438	0.404	0.427	0.527	0.500
Active Marrow						
Mass (kg)	0.047	0.150	0.320	0.610	1.050	1.120
Fraction[4]	0.134	0.132	0.118	0.132	0.137	0.112
Inactive Marrow						
Mass (kg)	-	0.020	0.140	0.590	1.550	2.380
Fraction[4]	-	0.018	0.052	0.127	0.203	0.238
Other tissues[5]						
Mass(kg)	0.164	0.469	1.154	1.453	1.022	1.5
Fraction[4]	0.467	0.412	0.426	0.314	0.133	0.150
Trabecular bone[6]						
Mass (kg)	0.140	0.200	0.219	0.396	0.806	1.000
Fraction[4]	0.176	0.438	0.081	0.085	0.105	0.100
S/V[7] (cm^2/cm^3)	-	220	-	225	-	190
Cortical bone[5]						
Mass (kg)	-	0.299	0.875	1.584	3.224	4.000
Fraction[4]	-	0.263	0.323	0.342	0.421	0.400
Surface Area (m^2)						
Trabecular	1.5	2.2	2.4	4.4	7.7	6.0
Cortical	-	0.45	1.3	2.4	4.8	6.0
Total	1.5	2.6	3.7	6.8	12	12

[1] See Ref. 26.
[2] See Ref. 27.
[3] Computed assuming 0.2 g-Ca per g bone mineral.
[4] Mass fraction in the skeleton.
[5] Difference between skeletal mass and identified tissues.
[6] All bone is trabecular at birth; 40% at one year, 20% thereafter.
[7] Surface to volume ratio, see Ref. 15.
[8] Based on trabecular bone mass and S/V ratio of 220 through age 10, 190 at age 15, and 120 for the adult.
[9] The adult S/V ratio for cortical bone was applied to all ages.

$n_r(T_i)dT_i$ denotes the number of electrons of energy between T_i and $T_i + dT_i$ liberated in region r per interaction i.

The mass ratios which appear in the equation can be related to the mean chord lengths of the trabeculae, $\langle t \rangle$, and marrow space, $\langle 1 \rangle$, as measured by scanning the trabeculation in an isotropic manner. The ratios expressed in terms of the measured chord-lengths are

$$\frac{m(TB)}{m(RM)} = \frac{\rho_{TB}}{\rho_{RM}} \frac{\langle t \rangle}{\langle 1 \rangle} \tag{8}$$

$$\frac{m(TB)}{m(BS)} = \frac{\rho_{TB}}{\rho_{RM}} \frac{\langle t \rangle}{4\ d} \tag{9}$$

$$\frac{m(RM)}{m(BS)} = \frac{\langle 1 \rangle}{4\ d} \tag{10}$$

where ρ_{TB} and ρ_{RM} denote the density of bone and marrow and d is the distance over which the endosteal tissue is averaged, i.e., in ICRP Publication 30 (20) a value of 10 μm is considered appropriate.

Soft-tissue adjacent to surfaces of trabecular bone represent about one half the total endosteal tissue of the skeleton. The remaining tissue is associated with the surfaces of cortical bone where it is contained within small cavities (largely the Haversian canals of about 50 μm diameter) within the bone matrix (17). The dose-response function for this component of the endosteal tissue is computed as

$$\frac{D(BS)}{\Phi(E)} = \int_0^\infty (i/\rho)_r\ n_r(T_i)\ T_i\ S(T_i)\ dT_i \tag{11}$$

where $S(T_i)$ denotes the ratio of the mass stopping power for soft tissue to that of bone at energy T_i. The total dose to endosteal tissues is the average of that indicated by Eqs. 7 and 11 since trabecular and cortical bone contribute about equally to the total endosteal tissue mass in the skeleton.

A complete set of dose response functions for the skeleton is given in Table 5 and those for the active marrow are shown in Fig. 4. These data can be applied to photon fluence estimates derived from Monte Carlo transport calculations in mathematical analogues of the body (1,26) to estimate absorbed dose. Variations with incident photon energy in the ratio of absorbed dose in active marrow to the equilibrium dose (kerma) in soft-tissue are indicated in Fig. 5. These ratios are maximal at photon energies in the region of 50 to 60 keV and are higher for the thick trabeculae and small marrow cavities of the parietal bone than for the thinner trabeculae-larger marrow cavities of other bones. The

Table 5. Absorbed dose in active marrow, D(RM), and in bone surface, D(BS), per unit fluence, $\Psi(E)$, of monoenergetic photons in the skeleton.

Photon energy (MeV)	D(RM or BS)/Ψ(E), Gy per photon/m^2					
	Parietal Bone		Lumber Vertebra		Cortical	Total[1]
	D(RM)	D(BS)	D(RM)	D(BS)	D(BS)	D(BS)
0.010	6.30(-16)	8.47(-16)	6.14(-16)	9.43(-16)	5.32(-15)	3.13(-15)
0.015	2.71(-16)	4.17(-16)	2.61(-16)	4.98(-16)	2.45(-15)	1.47(-15)
0.020	1.55(-16)	2.98(-16)	1.43(-16)	3.39(-16)	1.39(-15)	8.65(-16)
0.030	7.49(-17)	2.00(-16)	6.44(-17)	2.12(-16)	6.11(-16)	4.12(-16)
0.040	5.04(-17)	1.42(-16)	4.11(-17)	1.51(-16)	3.41(-16)	2.46(-16)
0.050	4.18(-17)	1.09(-16)	3.31(-17)	1.10(-16)	2.20(-16)	1.65(-16)
0.060	3.93(-17)	8.75(-17)	3.11(-17)	8.69(-17)	1.57(-16)	1.22(-16)
0.080	4.15(-17)	6.61(-17)	3.45(-17)	7.03(-17)	1.03(-16)	8.67(-17)
0.10	4.79(-17)	6.32(-17)	4.22(-17)	6.76(-17)	8.51(-17)	7.64(-17)
0.15	7.16(-17)	7.96(-17)	6.74(-17)	8.90(-17)	8.80(-17)	8.85(-17)
0.20	9.88(-17)	1.05(-16)	9.57(-17)	1.22(-16)	1.10(-16)	1.16(-16)
0.30	1.57(-16)	1.65(-16)	1.54(-16)	1.98(-16)	1.67(-16)	1.83(-16)
0.40	2.15(-16)	2.26(-16)	2.10(-16)	2.65(-16)	2.24(-16)	2.45(-16)
0.50	2.72(-16)	2.85(-16)	2.66(-16)	3.30(-16)	2.80(-16)	3.05(-16)
0.60	3.28(-16)	3.38(-16)	3.19(-16)	3.94(-16)	3.34(-16)	3.64(-16)
0.80	4.28(-16)	4.37(-16)	4.15(-16)	5.09(-16)	4.33(-16)	4.71(-16)
1.0	5.19(-16)	5.29(-16)	5.03(-16)	6.12(-16)	5.22(-16)	5.67(-16)
1.5	7.13(-16)	7.23(-16)	6.91(-16)	8.37(-16)	7.09(-16)	7.73(-16)
2.0	8.79(-16)	8.89(-16)	8.50(-16)	1.03(-15)	8.69(-16)	9.49(-16)
3.0	1.17(-15)	1.18(-15)	1.12(-15)	1.36(-15)	1.15(-15)	1.26(-15)
4.0	1.43(-15)	1.44(-15)	1.37(-15)	1.65(-15)	1.42(-15)	1.54(-15)
5.0	1.69(-15)	1.70(-15)	1.59(-15)	1.93(-15)	1.68(-15)	1.81(-15)
6.0	1.94(-15)	1.95(-15)	1.82(-15)	2.20(-15)	1.94(-15)	2.07(-15)
8.0	2.46(-15)	2.46(-15)	2.26(-15)	2.74(-15)	2.47(-15)	2.61(-15)
10.0	2.99(-15)	2.99(-15)	2.70(-15)	3.28(-15)	3.03(-15)	3.16(-15)

[1] Total represents the bone surface response of the skeleton and is computed as the average of the lumbar vertebra and cortical responses.

ORNL-DWG 84-14100

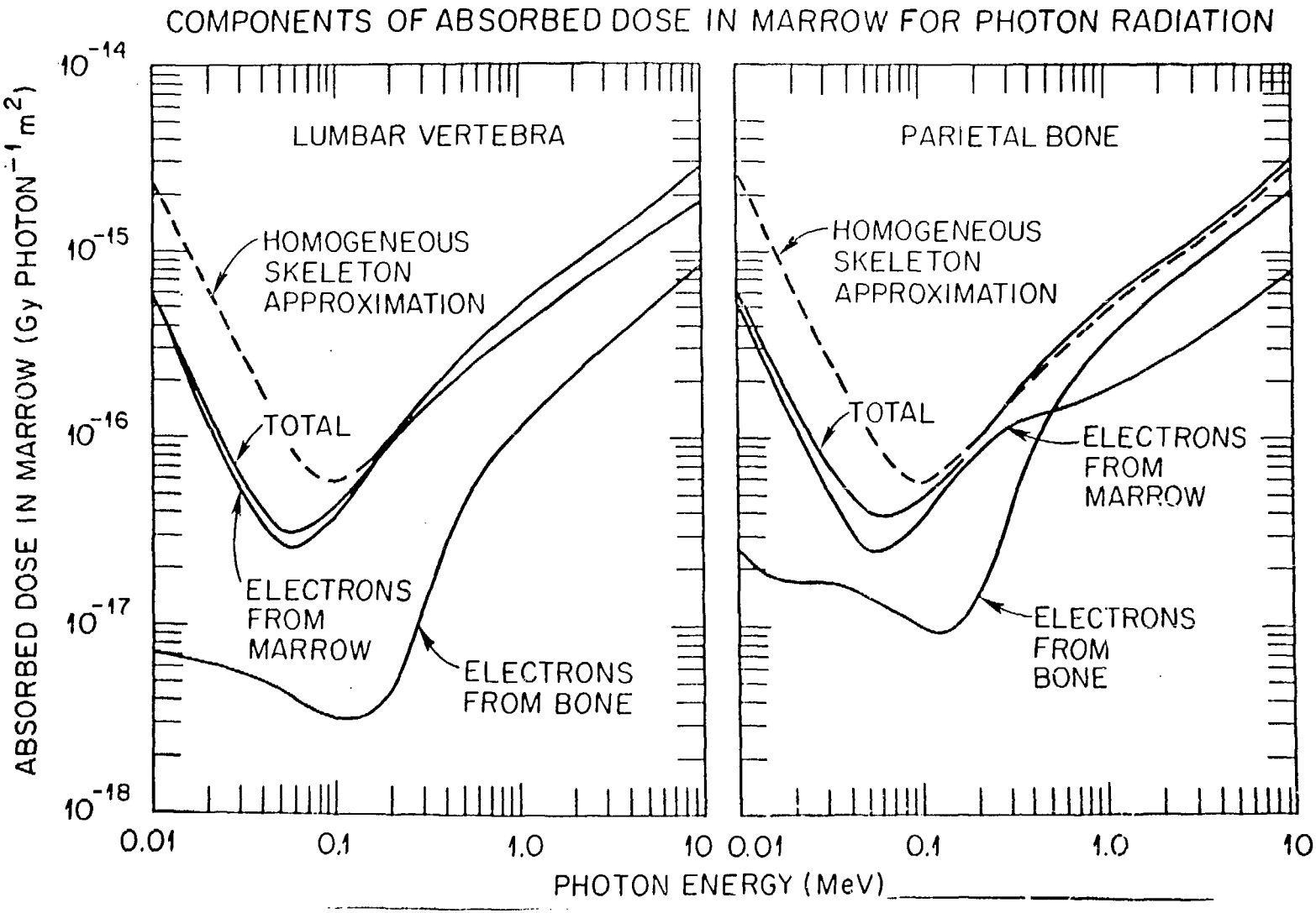

Figure 4. Components of the absorbed dose in marrow from photon radiations. The dotted curve assumes the active marrow absorbs energy per unit mass at the rate for the homogeneous skeleton approximation.

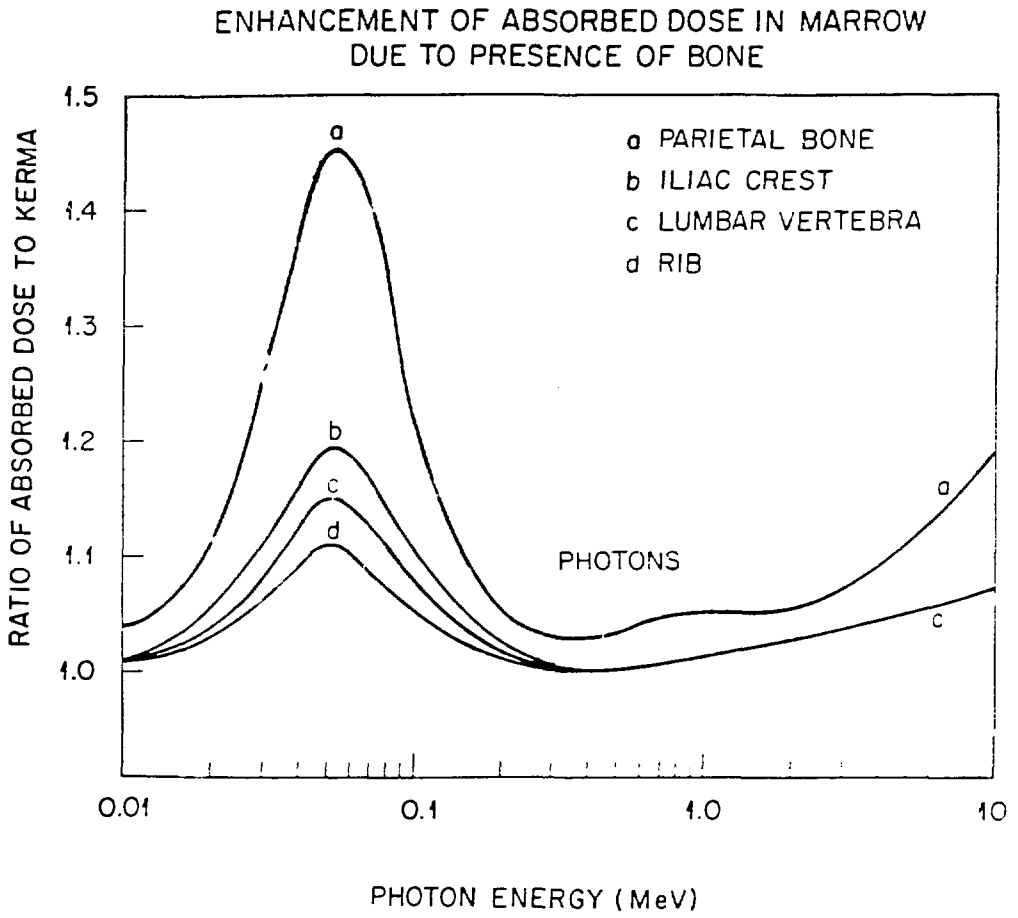

Figure 5. Illustration of the effects of the microstructure of trabecular bone on energy deposition in active marrow for various bones of the adult skeleton.

ratios at low energy conform to the general features indicated by Spiers (13). However, the parietal bone exhibits a substantially higher enhancement of the marrow dose than other trabecular bones. This enhancement should be considered in deriving skeletal average values for the diagnostic x-ray region. Enhancement of dose in the high energy (pair production) region is also indicated in our calculations. Enhancement is small, about 5%, for most trabecular sites but approaches 20% for the parietal bone. Considering the highly stylized analogue of the skeleton used in photon transport calculations, we recommend that the skull be treated as a separate bone region and data for the parietal bone in Table 5 be applied to estimate marrow dose. The lumbar vertebra appears to be representative of other trabecular sites.

this is more of a summary

DISCUSSION

Data on microstructure of trabecular bone has been used to estimate absorbed fractions for electrons in trabecular bone using a formulation similar to that set forth by Spiers (13). Absorbed fraction estimates are developed for electrons arising within the trabeculae or the marrow cavity itself. These data were applied to the secondary electrons arising from photon interactions within the skeleton in deriving dose-response functions which reflect the microstructure of trabecular bone. These functions overcome one of the well known limitations in current dosimetric formulations.

↑ it would be nice to briefly summarize this

ACKNOWLEDGMENT

Research sponsored by the Office of Health and Environmental Research, U.S. Department of Energy under contract DE-AC05-84OR21400 with the Martin Marietta Energy Systems, Inc.

REFERENCES

[1] Snyder, W. S., M. R. Ford, and G. G. Warner, "Estimates of Specific Absorbed Fractions For Photon Sources Uniformly Distributed In Various Organs of a Heterogeneous Phantom, Medical Internal Radiation Dose Committee, Pamphlet No. 5, Revised (Society of Nuclear Medicine, New York) 1978.

[2] Poston, J. W. and W. S. Snyder, "A model for exposure to a semi-infinite cloud of a photon emitter," Health Phys. 26, 287, 1974.

[3] Rosenstein, M., Organ Doses in Diagnostic Radiology, U.S. Department of Health, Education and Welfare Report FDA 76-8030 (Washington, DC: U.S. Government Printing Office) 1976.

[4] Spiers, F. W., "The influence of energy absorption and electron range on dosage in irradiated bone," Brit. J. Radiol. 12, 521, 1949.

[5] Spiers, F. W., "Dosage in irradiated soft tissue and bone," Brit. J. Radiol. 26, 38, 1953.

[6] Woodard, H. Q. and F. W. Spiers, "The effect of x rays of different qualities on the alkaline phosphates of living mouse bone," Brit. J. Radiol. 26, 38, 1953.

[7] Charlton, D. E. and D. V. Cormack, "Energy dissipation in finite cavities," Radia. Res., 17, 34, 1962.

[8] Aspin, N. and H. E. Johns, "The absorbed dose in cylindrical cavities within irradiated bone," Brit. J. Radiol. 36, 350, 1963.

[9] Howarth, J. L., "Calculation of the absorbed dose in soft-tissue cavities in bone irradiated by x-rays," Rad. Res. 24, 158, 1965.

[10] Kramer, R., Ermittlung von Konversionsfaktoren Zwischen Korperdosen und Relevanten Strahlungskenngrossen bei Externer Roentgen- und Gamma-Bremsstrahlung, Gesellschaft fur Strahlen-und Umweltforschung GSF-Bericht-S-566, 1979.

[11] Ashton, T. and F. W. Spiers, "Attenuation factors for certain tissues when the body is irradiated omnidirectionally," Phys. Med. Biol. 24, 950, 1979.

[12] Kerr, G. D., "A Review of organ doses from isotropic fields of γ-Rays," Health Phys. 39, 3, 1980.

[13] Spiers, F. W., "Transition-zone dosimetry," Radiation Dosimetry (edited by F. H. Attix and E. Tochlin) Vol. 3, pp. 809-867 (Academic Press; New York, N Y) 1969.

[14] Spiers, F. W., "Beta dosimetry in trabecular bone," Delayed Effects of Bone-Seeking Radionuclides (edited by C. W. Mays et al.) pp. 95-108 (U. of Utah Press; Salt Lake City, UT) 1969.

[15] Beddoe, A. H., P. J. Darley, and F. W. Spiers, "Measurements of trabecular bone structure in man," Phys. Med. Biol. 21, 589, 1976.

[16] Beddoe, A. H., "Measurements of the microscopic structure of cortical bone," Phys. Med. Biol. 22, 298, 1977.

[17] ICRP Publication 23, Report of the Task Group on Reference Man, Pergamon Press, Oxford, 1975.

[18] ICRP Publication 11, Task Group on Radiosensitivity of Tissues in Bone, Pergamon Press, Oxford, 1968.

[19] ICRP Publication 20, Alkaline Earth Metabolism in Adult Man, Pergamon Press, Oxford, 1972.

[20] ICRP Publication 30, Limits for Intakes of Radionuclides by Workers, (Pergamon Press: Oxford), 1979.

[21] Whitwell, J. R. and F. W. Spiers, "Calculated beta-ray dose factors for trabecular bone," Phys. Med. Biol. 21, 16, 1976.

[22] Spiers, F. W., J. R. Whitwell and A. H. Beddoe, "Calculated dose factors for radiosensitive tissues in bone irradiated by surface-deposited radionuclides," Phys. Med. Biol. 23, 481, 1978.

[23] Whitwell, J. R., Theoretical Investigations of Energy Loss by Ionizing Particles in Bone, Ph.D. Thesis, University of Leeds, Leeds, UK, 1973.

[24] Kellerer, A. M., "Consideration on the Random Traversal of Convex Bodies and Solutions for General Cyclinders," Radia. Res. 47, 359-376, 1971.

[25] Berger, M. J., "Improved Point Kernals for Electron and Beta-ray Dosimetry," NBSIR 73-107, 1973.

[26] Cristy, M., Mathematical Phantoms Representing Children of Various Ages for Use in Estimate of Internal Dose. NUREG/CR-1159, ORNL/NUREG/TM-367, 1980.

[27] Leggett, R. W., K. F. Eckerman, and L. R. Williams, "Strontium-90 in bone: A case study in age-dependent dosimetric modelling," Health Phys. 43, 307-322, 1982.